DOCTOR THESIS

Hydrostatic pressure under hypoxia facilitates
fabrication of tissue-engineered vascular grafts derived
from human vascular smooth muscle cells in vitro
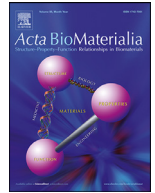
低酸素下における静水圧は in vitro における
ヒト血管平滑筋細胞由来の組織工学的人工血管の作製を促進する

March, 2024
（2024 年 3 月）

Tomoyuki Kojima
小嶋 朋之

Department of Obstetrics and Gynecology
Yokohama City University Graduate School of Medicine
横浜市立大学 大学院医学研究科 医科学専攻 生殖生育病態医学

(Doctoral Supervisor：Etsuko Miyagi, Professor)
（指導教員：宮城　悦子 教授）

Full length article

Hydrostatic pressure under hypoxia facilitates fabrication of tissue-engineered vascular grafts derived from human vascular smooth muscle cells *in vitro*

Tomoyuki Kojima [a,b,1], Takashi Nakamura [a,1], Junichi Saito [a], Yuko Hidaka [a], Taisuke Akimoto [c], Hana Inoue [a], Christian Nanga Chick [d], Toyonobu Usuki [d], Makoto Kaneko [e], Etsuko Miyagi [b], Yoshihiro Ishikawa [f], Utako Yokoyama [a,*]

[a] *Department of Physiology, Tokyo Medical University, Tokyo 160-0023, Japan*
[b] *Department of Obstetrics and Gynecology, Yokohama City University Graduate School of Medicine, Kanagawa 236-0004, Japan*
[c] *Department of Neurosurgery, Yokohama City University Graduate School of Medicine, Kanagawa 236-0004, Japan*
[d] *Department of Materials and Life Sciences, Faculty of Science and Technology, Sophia University, Tokyo 102-8554, Japan*
[e] *Graduate School of Science and Engineering, Meijo University, Aichi 468-8502, Japan*
[f] *Cardiovascular Research Institute, Yokohama City University Graduate School of Medicine, Kanagawa 236-0004, Japan*

ABSTRACT

Biologically compatible vascular grafts are urgently required. The scaffoldless multi-layered vascular wall is considered to offer theoretical advantages, such as facilitating cells to form cell-cell and cell-matrix junctions and natural extracellular matrix networks. Simple methods are desired for fabricating physiological scaffoldless tissue-engineered vascular grafts. Here, we showed that periodic hydrostatic pressurization under hypoxia (HP/HYP) facilitated the fabrication of multi-layered tunica media entirely from human vascular smooth muscle cells. Compared with normoxic atmospheric pressure, HP/HYP increased expression of N-myc downstream-regulated 1 (NDRG1) and the collagen-cross-linking enzyme lysyl oxidase in human umbilical artery smooth muscle cells. HP/HYP increased N-cadherin-mediated cell-cell adhesion via NDRG1, cell-matrix interaction (i.e., clustering of integrin $\alpha5\beta1$ and fibronectin), and collagen fibrils. We then fabricated vascular grafts using HP/HYP during repeated cell seeding and obtained 10-layered smooth muscle grafts with tensile rupture strength of 0.218–0.396 MPa within 5 weeks. Implanted grafts into the rat aorta were endothelialized after 1 week and patent after 5 months, at which time most implanted cells had been replaced by recipient-derived cells. These results suggest that HP/HYP enables fabrication of scaffoldless human vascular mimetics that have a spatial arrangement of cells and matrices, providing potential clinical applications for cardiovascular diseases.

Statement of significance

Tissue-engineered vascular grafts (TEVGs) are theoretically more biocompatible than prosthetic materials in terms of mechanical properties and recipient cell-mediated tissue reconstruction. Although some promising results have been shown, TEVG fabrication processes are complex, and the ideal method is still desired. We focused on the environment in which the vessels develop in utero and found that mechanical loading combined with hypoxia facilitated formation of cell-cell and cell-matrix junctions and natural extracellular matrix networks in vitro, which resulted in the fabrication of multi-layered tunica media entirely from human umbilical artery smooth muscle cells. These scaffoldless TEVGs, produced using a simple process, were implantable and have potential clinical applications for cardiovascular diseases.

---

* Corresponding author at: Department of Physiology, Tokyo Medical University, 6-1-1 Shinjuku, Shinjuku-ku, Tokyo 160-8402, Japan.
E-mail address: uyokoyam@tokyo-med.ac.jp (U. Yokoyama).
1 These authors contributed equally to this work.

1. Introduction

Cardiovascular disease is the leading global cause of death in adults, and it is expected to account for >22.2 million deaths worldwide by 2030 [1]. More than 60 % of cardiovascular disease is attributed to diseased vessels, including the coronary arteries, peripheral arteries, and large vessels [1]. Congenital cardiovascular disease affects approximately 1 % of living newborns and is a major cause of neonatal death [2]. Treatment of congenital cardiovascular disease with complex malformations, including absent, hypoplastic, or atretic portions of vessels, requires multiple surgeries and/or interventions. In adults, diseased vessels are replaced by autologous grafts or artificial vessels, and in pediatric patients, prosthetic vascular grafts are used to correct abnormal blood flow. However, there are limitations to these therapeutic strategies because of the limited number of healthy autologous grafts, thrombogenicity, and the lack of growth potential in pediatric patients [3,4]. Thus, biologically compatible tissue-engineered vascular grafts (TEVGs) are desired for both adult and pediatric patients.

The vascular walls have a highly organized layer structure that consists of multiple types of cells and extracellular matrices (ECMs), and a coordinated balance between cell-cell and cell-ECM adhesions is essential for the organization of individual cells into three-dimensional tissues [5]. Cell-cell adhesions are formed by the cadherin family of adhesion molecules, and the most common cell-ECM adhesions are mediated by integrins, which are linked to the internal cell cytoskeleton [5]. In addition, ECMs forming the physiological environment surrounding cells provide tissue-specific biomechanical properties and contribute to tissue integrity. Fully biological, scaffoldless TEVGs have the potential to provide these biomimetic microenvironments, allowing for a high degree of cell-cell and cell-matrix communications, both of which would maintain adequate ECM production [6,7]. Although a large body of evidence has recently emerged in support of TEVG technologies [7–10], a scaffoldless TEVG consisting of an organized spatial arrangement of cell-cell, cell-ECM, and ECM fibrils has not been reported.

During the fetal period, blood vessels, like other organs, develop in a hypoxic environment [11] and, especially when the vessels begin to be exposed to mechanical forces, the vascular smooth muscle layer thickens and ECMs are formed to withstand blood pressure [12]. Tissue engineering utilizing mechanical loading, including a bioreactor with perfusion [13–15] and hydrostatic pressurization [16,17], has been used with success to fabricate implantable scaffoldless TEVGs. However, the production of TEVGs usually involves a prolonged bioreactor cultivation period to achieve maturation of ECM and sufficient mechanical strength [18]. Hypoxic conditions have recently been introduced to the field of TEVGs [19,20]. The HIF-1α stabilizer-loaded electrospun polycaprolactone grafts enhanced endothelialization and vascular smooth muscle cell (VSMC) regeneration *in vivo* [19]. Culture of the human dermal fibroblast-seeded polycaprolactone scaffold under hypoxia shortened fabrication time to acquire strength for implantation [20]. Because it has been reported that a high amplitude of periodic hydrostatic pressure (HP) shortens the fabrication time of scaffoldless VSMC-derived TEVG [17], we investigated, in the present study, whether a supraphysiological range of HP combined with hypoxic conditions would facilitate the fabrication of TEVGs containing physiological cell-cell and cell-ECM adhesions and natural ECM network *in vitro*.

2. Materials and methods

2.1. Materials

Fibronectin, YC-1, chetomin, and echinomycin were purchased from Sigma-Aldrich (St. Louis, MO, USA). On-Target plus human NDRG1 (L-010563-00-0005), human CEBPA (L-006422-00-0005), human HIF1A (L-004018-00-0005) siRNA-SMARTpool and Non-targeting pool (D-001810-10-05) were purchased from Horizon Discovery (Cambridge, UK). Antibodies for fibronectin (#ab2413), HLA class 1 ABC (#ab70328), integrin α5 (#ab150361), integrin β1 (#ab30394), LOX (#ab31238), N-cadherin (#ab76057), CD45 (#ab10558), and NDRG1 (#ab37897) were purchased from Abcam (Cambridge UK). Antibodies for β-actin (#4970), C/EBPα (#2295), and Lamin A/C (#2032) were purchased from Cell Signaling Technology (Danvers, MA, USA). Antibodies for von Willebrand factor (#A0082) and calponin (#M3556) were purchased from Dako (Glostrup, Denmark). An antibody for SM1 (7600) was purchased from YAMASA (Chiba, Japan); an antibody for collagen alpha-1 (I) (#sc293182) was purchased from Santa Cruz Biotechnology (Dallas, TX, USA);, and an antibody for F-actin was purchased from Invitrogen (Carlsbad, CA, USA). Antibodies for mouse IgG, Alexa Fluor 488 (#A11034) and rabbit IgG, Alexa Fluor 546 (#A10040), and Hoechst 33258 solution were purchased from Invitrogen.

2.2. Isolation of human umbilical artery smooth muscle cells

We obtained human umbilical cords from Yokohama City University Hospital, Japan. Three human umbilical cords from normal term deliveries were utilized for this study. All pregnant women signed written informed consent. All procedures were approved by the human subject committees of the Yokohama City University School of Medicine (Reference number: A170126002, Approval date: 12/27/2019) and Tokyo Medical University (Reference number: T2019-0218, Approval date: 02/28/2020) and were conducted in accordance with the ethical principles of the Declaration of Helsinki.

The umbilical arteries were separated from the umbilical cords. Adventitial tissues were removed with forceps, and the tunica media was cut into 1-mm^2 pieces. The pieces were placed on culture dishes, and glass pieces were placed on top to prevent them from floating away. The pieces of umbilical arteries were cultured in Dulbecco's Modified Eagle Medium (DMEM) containing 10 % fetal bovine serum (FBS), 100 U/mL penicillin, and 100 mg/mL streptomycin for 3 weeks. Isolated human umbilical artery smooth muscle cells (hUASMCs) were cultured in a moist tissue culture incubator at 37 °C in 5 % CO_2 ambient air.

2.3. Periodic hydrostatic pressure system

We utilized a culturing system as previously described [17]. Briefly, this system comprised a pressure chamber, an incubator, a compressor, a flow regulator, and an air tank (JH0133, Koganei Corp., Tokyo, Japan). The compressor inlet is connected to the multi-gas incubator (Astec, Fukuoka, Japan) containing air at 37 °C with 5 % CO_2, and the outlet is connected to the air tank. Once the air in the incubator is collected in the air tank, pressurized air is supplied to the pressure chamber by regulating the flow from the air tank. We applied biphasic pressure to cultured cells, which enabled circulation of fresh air with 5 % CO_2 into the pressure chamber during hydrostatic pressure (HP) treatment. The pressure chamber was placed inside the incubator and kept at 37 °C during the experiments. The oxygen concentration in the pressure chamber can be changed by changing the oxygen concentration in the incubator.

2.4. Cell culture and treatment of hUASMCs

hUASMCs isolated from the umbilical artery were used to fabricate multi-layered cell sheets. For the mono-layered cell assay, isolated hUASMCs were used for RNA-sequencing, and hUASMCs

obtained from ScienCell (Carlsbad, CA, USA) were used for quantitative PCR, western blotting, and immunocytochemistry. We used a culturing system in which cells were cultured with periodic HP under various degrees of partial oxygen pressure. Cells were exposed to four different stimulations: (1) AP/NOR: atmospheric pressure (101 kPa) under normoxia (PO_2 = 140 mmHg; 5 % CO_2 and 95 % humidified air); (2) HP/NOR: hydrostatic pressure (110–180 kPa, 0.002 Hz) under normoxia (PO_2 = 140 mmHg; 10 % O_2, 5 % CO_2, and 85 % N_2) (Fig. S1A); (3) AP/HYP: atmospheric pressure (101 kPa) under hypoxia (PO_2 = 70 mmHg; 3 % O_2, 5 % CO_2, and 92 % N_2); and (4) HP/HYP: hydrostatic pressure (110–180 kPa, 0.002 Hz) under hypoxia (PO_2 = 70 mmHg; 1 % O_2, 5 % CO_2, and 94 % N_2) (Fig. S1B). YC-1 (30 μM), chetomin (100 nM), and echinomycin (30 nM) were administered for 1 h before and during stimulations.

2.5. Immunocytochemistry

hUASMCs were fixed in 10 % buffered formalin for 5 min and subjected to immunocytochemistry. Immunocytochemical analysis was performed as previously described [17]. Briefly, fixed cells were washed twice with PBS and permeabilized in 0.1 % Triton X-100 for 10 min. Cells were incubated with 1 % BSA/Tween 20/PBS for 20 min and then incubated with primary antibodies at 4 °C for 18 to 36 h. Cells were then incubated with a secondary antibody Alexa Fluor 488 goat anti-mouse IgG and Alexa Fluor 546 donkey anti-rabbit IgG for 1 h. DNA was stained with Hoechst 33258 solution. Images were obtained with a confocal microscope (LSM710, Zeiss, Oberkochen, Germany). The fluorescence intensity of three representative images was assessed and then averaged.

2.6. Bulk RNA-sequencing

hUASMCs isolated from two umbilical cords were treated for 24 h. Total RNA was isolated using the RNeasy Mini Kit (Qiagen, Venlo, the Netherlands). The concentration and quality of RNAs were assessed by a Nanodrop ND-2000 Spectrometer (ThermoFisher Scientific, Waltham, MA, USA). Collected RNAs were transferred to Riken Genesis Co. Ltd. (Kawasaki, Japan), where RNA libraries were built using a TruSeq RNA Sample Prep Kit v2 (Illumina, San Diego, CA, USA) and sequenced in accordance with the manufacturer's protocol.

Gene-set enrichment analyses (GSEAs) were conducted to investigate the functions of genes that significantly correlated with HP/HYP. GSEA ranks the gene list by the correlation between genes and phenotype and calculates an enrichment score to assess the gene distribution. Each analysis was performed 1000 times permutation, using the expression of HP/HYP as a phenotype label. Gene sets were considered significantly enriched if the false discovery rate (FDR) *q* value was <0.25 [21].

2.7. Quantitative real-time polymerase chain reaction

RNA isolation, cDNA synthesis, and real-time quantitative PCR (RT-PCR) were performed using protocols described previously [17]. The oligonucleotides used for RT-PCR are listed in Table S1. The abundance of each gene was calculated relative to the internal control of 18S RNA transcripts.

2.8. Western blotting

Whole-cell lysates were retrieved using a lysis buffer. Nuclear fractions of cultured cells were prepared using NE-PER Nuclear and Cytoplasmic Extraction Reagents in accordance with the manufacturer's instructions (ThermoFisher Scientific). Proteins were separated by SDS-PAGE and transferred to a polyvinylidene difluoride membrane by electroblotting. Membranes were blocked in TBS-0.1 % 20 containing 5 % skim milk and incubated with primary antibody at 4 °C overnight, and then incubated with peroxidase-linked secondary antibodies for 1 h. Specific binding was visualized by WSE-6200HL LuminoGraphII (ATTO, Tokyo, Japan).

2.9. siRNA transfection

For transient transfection with small interfering (si)RNA, 40–60 % confluent hUASMCs were prepared and transfected with *NDRG1*-targeted (8 nM), *CEBPA*-targeted (25 nM), or *HIF1A*-targeted (25 nM) siRNA using Lipofectamine RNA iMAX (Invitrogen) diluted in Opti-Mem I Reduced-Serum Medium (Gibco, Carlsbad, CA, USA) according to the manufacturer's instructions. The negative control was performed using siRNA of non-targeting at the same concentration of siRNA of the target.

2.10. ELISA

Cell lysates were retrieved using a lysis buffer, and protein expression was determined by Human/Mouse Total HIF-1 alpha/HIF1A DuoSet IC ELISA (R&D System, Minneapolis, MN, USA) according to the manufacturer's instructions.

2.11. Quantification of total collagen production

Cell culture supernatant was concentrated using concentrating solution (#90626, Chondrex, Redmond, WA, USA), and the amount of total collagen was quantified using Sirius Red Total Collagen Detection Assay Kit (#9062, Chondrex) according to the manufacturer's instructions. The absorbance of the extracted solution was read by Powerscan HT (Agilent, Santa Clara, CA, USA). Total collagen contents were calculated based on the standard curve.

2.12. Fabrication of multi-Layered hUASMC sheets by pressurization under hypoxia

To fabricate the first layer of the multi-layered cell sheets, hUASMCs were seeded on a fibronectin-coated atelocollagen membrane (diameter, 26 mm, Koken, Tokyo, Japan) at a density of 6.0×10^5 cells per dish (1130 cells/mm^2). Twenty-four hours after seeding, the cells were exposed to HP/HYP for 24 h. The cells for the next layer were then seeded on the first layer. This cell seeding and HP/HYP exposure were repeated 10 times to fabricate a 10-layered sheet. The 10-layered sheet was incubated in culture medium with ascorbic acid (AA2G, 50 μg/mL; Tokyo Chemical Industry, Tokyo, Japan) under AP/NOR for 1 week, and then detached from an atelocollagen membrane using a cell scraper and wrapped around a glass mandrel (diameter, 1.0 mm). The wrapped 10-layered sheet was incubated in culture medium with ascorbic acid for 1 additional week. After incubation, the glass mandrel was removed. A period of 34 days was required to fabricate arterial grafts derived from hUASMCs.

2.13. Characterization of hUASMC sheets

2.13.1. Transmission electron microscopy

Three-layered hUASMC sheets were fixed in half-strength Karnovsky's fixative (2.5 % glutaraldehyde and 2.0 % paraformaldehyde in 0.1 M phosphate buffer, pH 7.4) for 2 h at 4 °C. After washing in 0.1 M phosphate buffer twice, the specimens were fixed in 1 % osmium tetroxide for 2 h at 4 °C. Post-fixation, they were dehydrated using graded ethanol, substituted using n–butyl glycidyl ether for 15 min twice, and in a mixture of equal parts of QY-1 and epoxy resin. Next, they were embedded in epoxy resin for 3 h at room temperature. They were placed in an embedding plate filled

with new epoxy resin and polymerized in an incubator at 60 °C for 3 days. Ultra-thin sections (90-nm thick) were put on copper reseaux after staining with gadolinium acetate for 20 min at room temperature and stained with Reynold's lead citrate for 10 min at room temperature and examined by JEM-1400Flash (Japan Electron Optics Laboratory, Tokyo, Japan).

2.13.2. Scanning electron microscopy

Three-layered hUASMC sheets were fixed in half-strength Karnovsky's fixative at 4 °C overnight. The specimens were post-fixed in 1 % osmium tetroxide and placed in 1 % aqueous solution of tannic acid. They were dehydrated with graded concentrations of ethanol, immersed in *tert*–butyl alcohol, and then dried by the *tert*–butyl alcohol freeze-drying method. The specimens were then sputter-coated with gold and examined using a Hitachi S-2300 scanning electron microscope (Tokyo, Japan).

2.13.3. Surface plots analysis

The 3-dimensional surface plots of multi-layered cell sheets were performed using the "interactive 3D surface plot" plugin preloaded in Image J (National Institutes of Health, Bethesda, MD, USA). This plugin converted the pixel values into height information.

2.13.4. Mechanical test

The tensile rupture strength of the tubular hUASMC graft was determined using a DMT560 tissue puller (Danish MyoTechnology, Hinnerup, Denmark) as described previously [17]. Two parallel steel hooks were set inside a tubular graft segment (length, 3.5 mm), which was pulled until complete rupture at a speed of 100 μm/s. The force and displacement were recorded. Tensile rupture strength is determined by peak force/tissue cross-sectional area. Elastic moduli of the grafts were calculated using each plot's initial linear region spanning 2.5–4.0 strain, because all stress–strain data plots were linear ($R^2 \geq 0.90$) in the 2.5–4.0 strain region (Table S2).

2.14. Tissue staining and immunohistochemistry

Paraffin-embedded blocks were cut into 4-μm-thick sections and placed on glass slides. Hematoxylin and eosin (HE) staining was used to measure the thickness of 5-layered cell sheets. The measurement was performed using 3 representative images per sample and then averaged. Elastica van Gieson stain and picrosirius red stain were performed with standard protocols, and the amounts of elastin and collagen fibers were quantified using ImageJ. Implantation site and native aorta on the same sections were measured in each of 4 representative images and averaged. The sections stained with picrosirius red stain were imaged under polarized light to evaluate type I and III collagen deposition.

For immunohistochemistry, the sections were de-paraffinized, rehydrated, and incubated with primary antibodies at 4 °C for 18–36 h. The sections were incubated for 30 min in biotinylated second antibodies (Vectastain Elite ABC IgG kit, Vector Labs, Burlingame, CA, USA). The targeted proteins were visualized using DAB (Dako). The sections were counterstained with Mayer's hematoxylin. The negative control was confirmed by omission of primary antibodies. To evaluate the presence of hUASMCs in the rat aorta, the expression of HLA class I ABC was quantified using ImageJ.

For immunofluorescent staining, de-paraffinized sections were incubated with primary antibodies at 4 °C overnight. After 3 washes with Tween 20/PBS, the sections were incubated with secondary antibodies, Alexa Fluor 488 goat anti-mouse IgG, and Alexa Fluor 546 donkey anti-rabbit IgG for 1 h. After 6 washes with Tween 20/PBS, DNA was stained with Hoechst 33258 solution. After 2 washes with PBS, coverslips were mounted for microscopic imaging.

2.15. Implantation

Male nude rats (F344/NJcl–rnu/rnu, 200–250 g body weight) were used for the implantation of hUAMSC grafts. All animal experiments were approved by the Institutional Animal Care and Use Committee at Yokohama City University (F-A-16-009) and Tokyo Medical University (R4-078). Rats were anesthetized in a closed chamber with 4 % isoflurane. Anesthesia was maintained with 1.5–2.5 % isoflurane by mask. A graft (1.5 × 1.0 mm or 4.0 × 1.0 mm) was sutured at the infrarenal aorta, in which a section (the same size as the graft) of the aortic vessel wall was completely resected, as previously shown [17]. Immediately after surgery, rats were injected with the antibiotic enrofloxacin (5 mg/kg; Bayer, Leverkusen, German). One week, 3 weeks, 3 months, and 5 months after surgery, laparotomy was performed for histological evaluation of the implantation site. As a control, an expanded polytetrafluoroethylene (ePTFE) graft implantation (Gore & Associates GK, Tokyo, Japan) was performed in the same manner as above; 3 weeks after surgery, the implantation site was analyzed by the histological method.

2.16. Echocardiography

Rats were anesthetized in a closed chamber with 4 % isoflurane. Anesthesia was maintained with 1.5–2.5 % isoflurane by mask, and rats underwent ultrasonography (model SSA-700A, Diagnostic Ultrasound System, Toshiba, Tokyo, Japan). Pulsed Doppler blood velocity was measured across the junction between the distal end of the patch graft and the native aorta.

2.17. Statistical analysis

Data are presented as medians (interquartile range). Comparisons between 2 groups were made with Mann–Whitney *U*-tests, and multiple groups were compared by Kruskal–Wallis test followed by Fisher least significant difference post hoc test, Mann–Whitney test. A value of $P < 0.05$ was considered statistically significant.

3. Results

3.1. Periodic hydrostatic pressurization under hypoxia increases cell-cell adhesion through NDRG1

We first examined the effect of HP/HYP (110–180 kPa; 0.002 Hz; a time ratio of 1:1 between high and low pressure; 70 mmHg of partial oxygen pressure) on cell-cell adhesion by using the pressurization culture system [7,16,17] (Fig. S1) in hUASMCs, and found that N-cadherin, which mainly regulates VSMC cell-cell adhesion [22], was increased at the junctions of hUASMCs cultured with HP/HYP compared with AP/NOR (Fig. 1A).

To examine the molecular mechanisms underlying the increase in N-cadherin expression on the cell membrane, we performed RNA-sequencing using hUASMCs cultured under HP/HYP, AP/NOR, AP/HYP, or HP/NOR conditions for 24 h. The expression of 20 genes was increased more than 2-fold by HP/HYP compared with AP/NOR (Table S3). Among these genes, we focused on N-myc downstream-regulated gene-1 (*NDRG1*), which has been reported to enhance membrane expression of the adherence junction components E-cadherin and β-catenin [23]. In accordance with the previous reports [24], hypoxia *per se* (AP/HYP) induced *NDRG1* upregulation, and HP/HYP-induced *NDRG1* expression was significantly greater
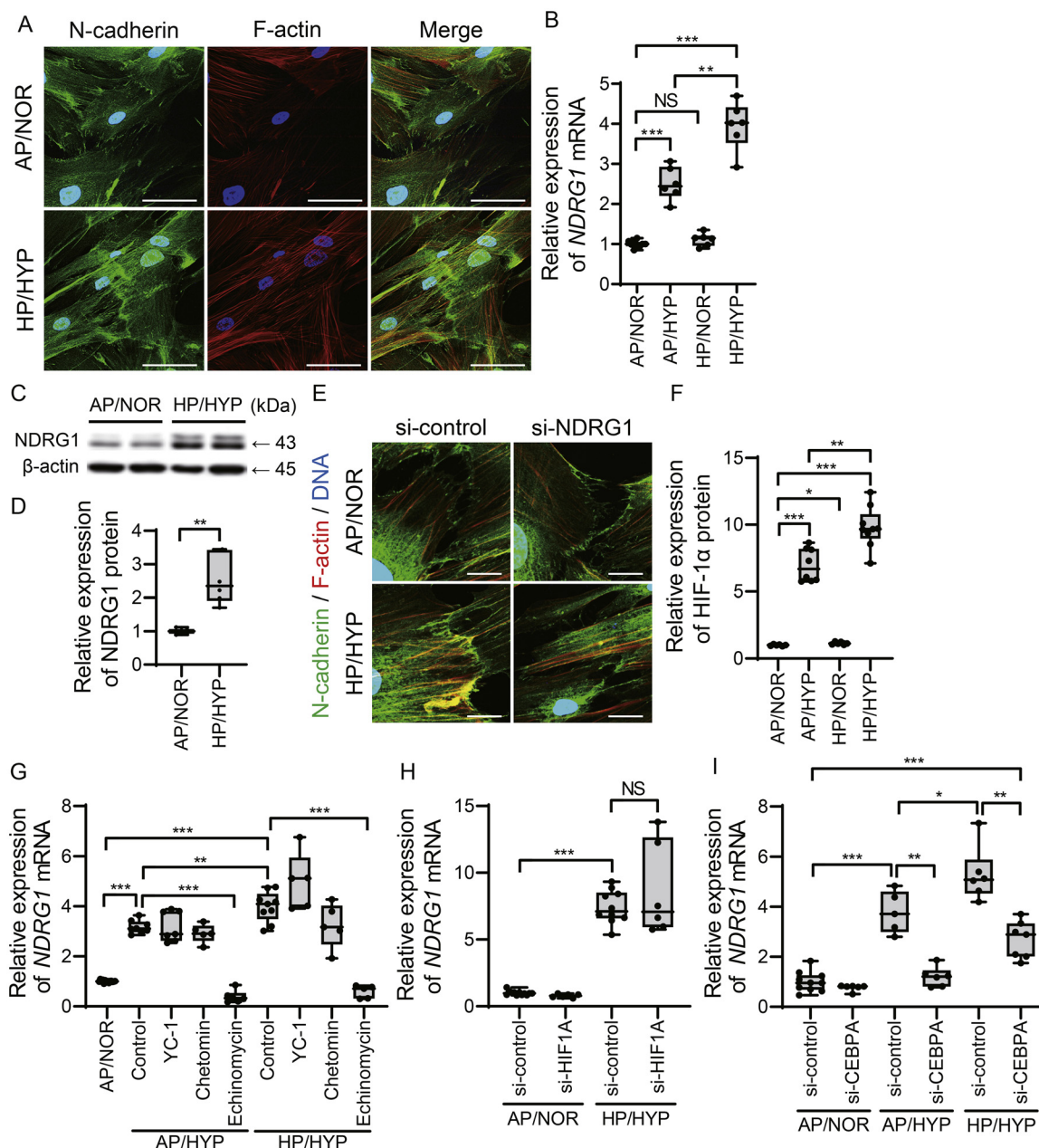
Fig. 1. HP/HYP increased N-cadherin-mediated cell-cell adhesion through the C/EBPα–NDRG1 pathway in hUASMCs. (A) Representative images of immunocytochemistry of hUASMCs cultured with AP/NOR or HP/HYP for 24 h. Cells were stained for N-cadherin (green), F-actin (red), and DNA (blue). Scale bars: 50 μm. (B) Expression of *NDRG1* mRNA in hUASMCs cultured with AP/NOR, AP/HYP, HP/NOR, or HP/HYP for 24 h; $n = 6$–9. (C) Representative blots of NDRG1 and β-actin proteins in hUASMCs cultured with AP/NOR or HP/HYP for 24 h. (D) Quantification of (C); $n = 6$. (E) Representative images of immunocytochemistry of hUASMCs transfected with *NDRG1*-targeted siRNA or control siRNA cultured with AP/NOR or HP/HYP for 24 h. hUASMCs were stained for N-cadherin (green), F-actin (red), and DNA (blue). Scale bars: 20 μm. (F) HIF-1α protein expression was measured by ELISA in hUASMCs cultured with AP/NOR, AP/HYP, HP/NOR, or HP/HYP for 6 h; $n = 6$–9. (G) Expression of *NDRG1* mRNA in hUASMCs treated with YC-1 (30 μM), chetomin (100 nM), or echinomycin (30 nM) cultured with AP/NOR, AP/HYP, or HP/HYP for 24 h; $n = 5$–14. (H) Expression of *NDRG1* mRNA in hUASMCs transfected with *HIF1A*-targeted siRNA or control siRNA cultured with AP/NOR or HP/HYP; $n = 6$–12. (I) Expression of *NDRG1* mRNA in hUASMCs transfected with *CEBPA*-targeted siRNA or control siRNA cultured with AP/NOR, AP/HYP, or HP/HYP; $n = 5$–10. NS, not significant, $^*P < 0.05$, $^{**}P < 0.01$, $^{***}P < 0.001$. Boxes represent the medians and interquartile range; whiskers indicate the minimum to maximum values. (For interpretation of the references to color in this figure legend, the reader is referred to the web version of this article.)

than AP/HYP- or HP/NOR-induced *NDRG1* expression (Fig. 1B). Additionally, we examined the effects of amplitude and frequency of HP and the ratio of time between high and low pressure on *NDRG1* expression. Hydrostatic pressurization at 110–180 kPa with a cycle of 0.002 Hz and a time ratio of 1:1 between high and low pressure was most effective in increasing *NDRG1* expression (Fig. S2A–C). HP/HYP-induced NDRG1 upregulation was also observed at the protein level (Fig. 1C and D). *NDRG1*-targeted siRNA decreased

NDRG1 mRNA by approximately 80 % (Fig. S3A and B) and attenuated HP/HYP-induced N-cadherin membrane localization at cell junctions (Fig. 1E).

3.2. C/EBPα, not HIF-1α, is involved in NDRG1 upregulation

Because hypoxia-inducible factor 1 alpha (HIF-1α) binds to the *NDRG1* promoter to activate *NDRG1* expression [24], we quan-
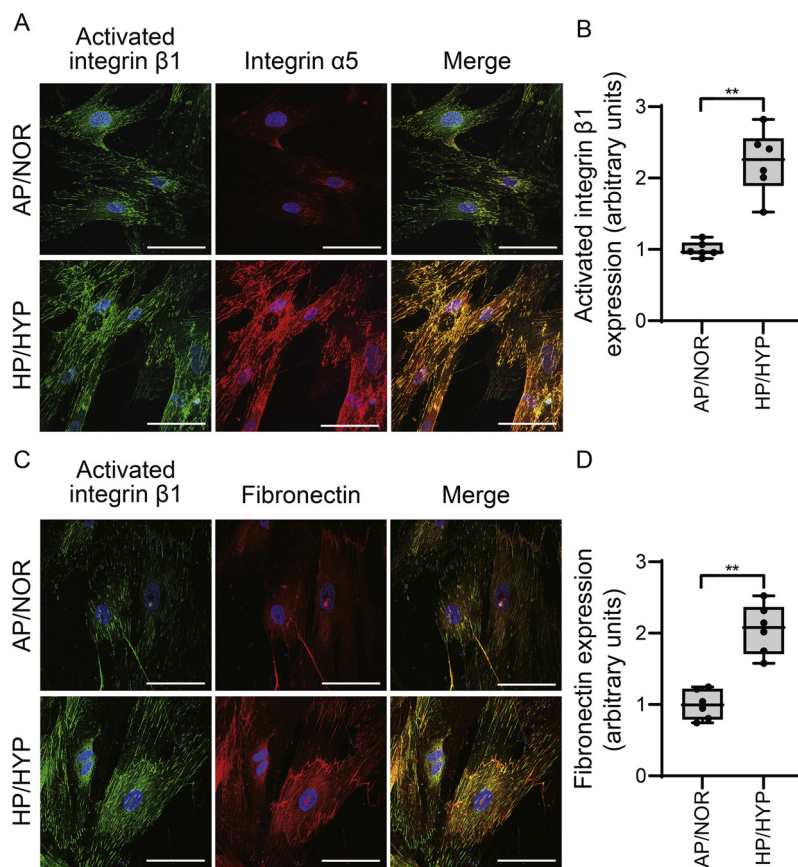
Fig. 2. HP/HYP increased expression of integrin $\alpha5\beta1$ and fibronectin fibrillogenesis in hUASMCs. (A) Representative images of immunocytochemistry of hUASMCs cultured with AP/NOR or HP/HYP for 24 h. hUASMCs were stained for activated integrin $\beta1$ (green), integrin $\alpha5$ (red), and DNA (blue). Scale bars: 50 μm. (B) Semiquantification of the intensity of activated integrin $\beta1$; $n = 6$. (C) Representative images of immunocytochemistry of hUASMCs cultured with AP/NOR or HP/HYP for 24 h. hUASMCs were stained for activated integrin $\beta1$ (green), fibronectin (red), and DNA (blue). Scale bars: 50 μm. (D) Semiquantification of the intensity of fibronectin; $n = 6$. **P < 0.01. Boxes represent the medians and interquartile range; whiskers indicate the minimum to maximum values. (For interpretation of the references to color in this figure legend, the reader is referred to the web version of this article.)

tified HIF-1α protein expression. Both AP/HYP and HP/HYP increased HIF-1α protein, and HP/HYP-induced HIF-1α expression was greater than AP/HYP-induced HIF-1α expression (Fig. 1F); however, the HIF-1α inhibitors YC-1 and chetomin and silencing of *HIF1A* did not affect HP/HYP-induced *NDRG1* upregulation (Fig. 1G and H and Fig. S3C and D). In contrast, the HIF-1α inhibitor echinomycin, which also inhibits CCAAT enhancer binding protein alpha (C/EBPα) encoded by *CEBPA* [25], significantly inhibited HP/HYP-induced *NDRG1* expression. Silencing of *CEBPA* significantly inhibited HP/HYP-induced *NDRG1* upregulation (Fig. 1I and Fig. S3E–G). These data suggest that, at least in part, C/EBPα is involved in HP/HYP-mediated *NDRG1* upregulation.

3.3. Periodic hydrostatic pressure under hypoxia increased cell-matrix adhesion

Cell-matrix adhesion is required for organized tissue structure, and the connection between integrins and fibronectin results in fibronectin fibrillogenesis, which is the critical step for several scaffold ECMs, including collagen and elastic fibers [26]. We investigated the effect of HP/HYP on the expression of integrin $\beta1$ and $\alpha5$, the major integrin subtypes for fibronectin binding. HP/HYP significantly increased activated integrin $\beta1$, which co-localized with integrin $\alpha5$ (Fig. 2A and B). Fibronectin fibrillogenesis was promoted in cultured hUASMCs with HP/HYP compared to AP/NOR (Fig. 2C and D).

3.4. Periodic HP/HYP has potential for promoting collagen fibril formation via HIF-1α

To investigate whether HP/HYP has the potential to fabricate a spatial ECM network *in vitro*, we performed Gene Ontology analysis using the previously mentioned RNA-sequencing data. A positive correlation between HP/HYP and the ECM-related gene set GOCC_COLLAGEN_TRIMER was detected, and multiple collagen subtypes and lysyl oxidase (LOX), which is an essential enzyme for cross-linking of collagens and ordered collagen fibrinogenesis [27,28], were increased in hUASMCs cultured with HP/HYP compared to AP/NOR (Fig. 3A and Table S4). The expression of *COL1A1*, which plays a role in imparting strength to the vessel wall [12], was most increased by HP/HYP compared with the other conditions (AP/HYP and HP/NOR) (Fig. 3B). Although the degree of increase in *COL1A1* mRNA was modest, total collagen production was markedly increased by HP/HYP (Fig. 3C).

The expression of *LOX* was most increased by HP/HYP compared with the other conditions (Fig. 3D), and the level of LOX protein expression was also increased by HP/HYP (Fig. 3E and F). HP/HYP-induced LOX expression was significantly inhibited by the HIF-1α inhibitors YC-1, chetomin, and echinomycin, suggesting that this LOX upregulation is mediated by HIF-1α (Fig. 3G). Among various HP conditions, 110–180 kPa with a cycle of 0.002 Hz and a time ratio of 1:1 between high and low pressure was most effective in increasing *LOX* expression; these conditions were the same as those suitable for *NDRG1* upregulation (Fig. S2D–F).
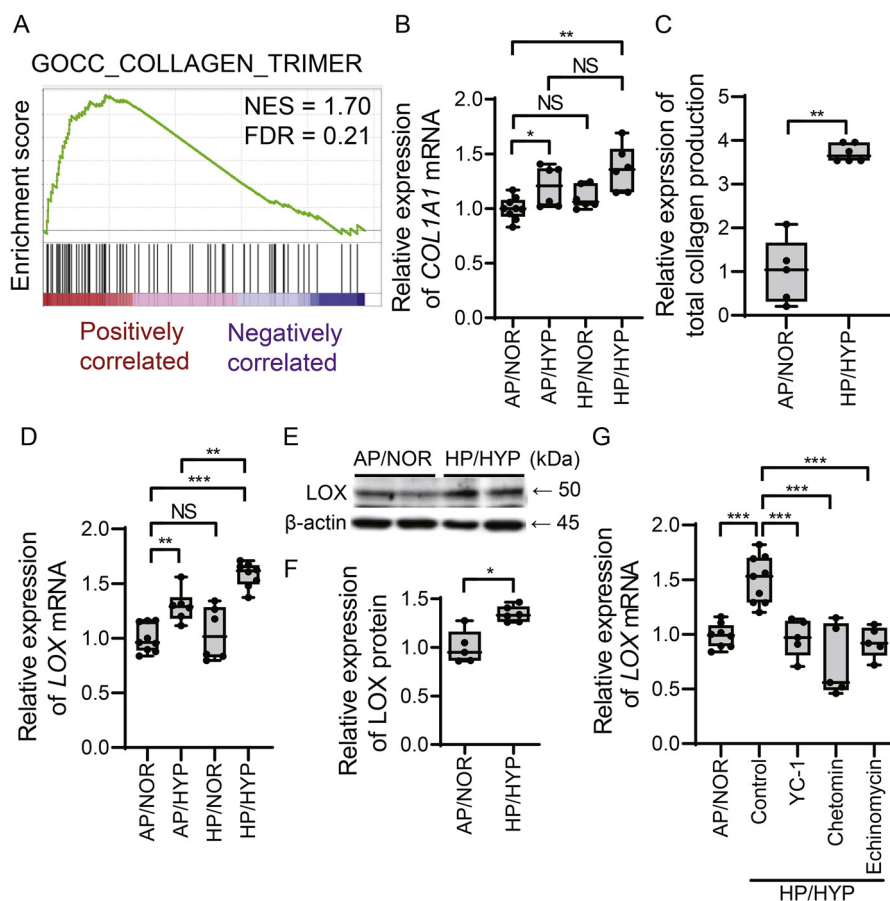
Fig. 3. HP/HYP promoted collagen secretion and increased LOX expression through HIF-1α in hUASMCs. (A) GSEAs revealed a positive correlation between hUASMCs cultured with HP/HYP for 24 h and collagen-related gene sets (GOCC_COLLAGEN_TRIMER). On the x-axis, the genes in each gene set are ranked from the left side (positively correlated) to the right side (negatively correlated). The vertical black lines indicate each gene in the gene set. The green line indicates the enrichment score of each gene. NES and FDR indicate normalized enrichment score and false discovery rate, respectively. (B) Expression of *COL1A1* mRNA in hUASMCs cultured with AP/NOR, AP/HYP, HP/NOR, or HP/HYP for 24 h; $n = 6$–9. (C) Relative expression of total collagen production in hUASMCs cultured with AP/NOR or HP/HYP for 24 h; $n = 5$–6. (D) The expression of *LOX* mRNA in hUASMCs cultured with AP/NOR, AP/HYP, HP/NOR, or HP/HYP for 24 h; $n = 6$–9. (E) Representative blots of LOX and β-actin proteins in hUASMCs cultured with AP/NOR or HP/HYP for 24 h. (F) Quantification of (E); $n = 5$–6. (G) The expression of *LOX* mRNA in hUASMCs treated with YC-1 (30 μM), chetomin (100 nM), or echinomycin (30 nM) cultured with AP/NOR or HP/HYP for 24 h; $n = 5$–9. NS, not significant, $^*P < 0.05$, $^{**}P < 0.01$, $^{***}P < 0.001$. Boxes represent the medians and interquartile range; whiskers indicate the minimum to maximum values. (For interpretation of the references to color in this figure legend, the reader is referred to the web version of this article.)

Using other cell types, we assessed whether the HP/HYP-induced upregulation of *NDRG1* and *LOX* were specific for hUASMCs. HP/HYP significantly increased both *NDRG1* and *LOX* mRNA expression, to varying degrees, in all cell types tested, such as human aortic and pulmonary artery VSMCs, human dermal and lung fibroblasts, and endothelial cells (Fig. S4). Thus, HP/HYP-mediated upregulation of *NDRG1* and *LOX* appears to be a general rather than cell type–specific mechanism.

3.5. Fabrication of multi-layered human VSMC sheet by HP/HYP culture

Based on these findings showing the potential of HP/HYP culture conditions to fabricate cell-cell and cell-matrix adhesions and spatial ECM network *in vitro* without the use of exogenous scaffold materials, we performed repeated cell seeding and HP/HYP culture according to the protocol shown in Fig. S5. Transmission electron microscopic analyses revealed the presence of adherence junctions in 3-layered hUASMC sheets cultured with HP/HYP but not with AP/NOR (Fig. 4A). Scanning electron microscopy demonstrated tightly aligned VSMCs in the 3-layered hUASMC sheets cultured with HP/HYP, whereas the cell sheets cultured with AP/NOR had gaps between cells (Fig. 4B). Although cell-cell adhesions were formed to some extent in the cell sheets fabricated using AP/HYP

and HP/NOR, the degrees of cell-cell adhesions were less than in the cell sheets cultured with HP/HYP (Fig. 4A and B). hUASMCs were stably stacked up to 10 layers in HP/HYP culture, but cells aggregated after 4 layers and did not form cell sheets under AP/NOR conditions (Fig. 4C). hUASMCs treated with echinomycin, which was shown to inhibit increases in *NDRG1* and *LOX* expression, did not form cell sheets in HP/HYP (Fig. 4D–F).

The 10-layered VSMC sheets were easily detached from the culture apparatus and wrapped around glass rods (Fig. 4G). Immunofluorescence revealed that the multi-layered hUASMC sheets contained collagen type I alpha 1 and fibronectin (Fig. 4H). Elastica van Gieson stain failed to detect layered elastic lamella in hUASMC sheets (Fig. S6), whereas mass spectrometry detected desmosine and isodesmosine, which are LOX-mediated cross-linking amino acids of elastin [29], in hUASMC sheets (Table S5). These data suggest activation of LOX in hUASMC sheets. The ringlets of tubular hUASMC sheets were pulled under tension to rupture (Fig. 4I and Movie S1). Stress–strain curves from hUASMC sheets are shown in Fig. 4J. The tensile rupture strength of the hUASMC sheets was 0.278 (0.247–0.279) MPa, corresponding to 2092 (1855–2095) mmHg. The elastic moduli of hUASMC sheets were 0.090 (0.084–0.114) MPa (Table S2). Tensile rupture strengths of the hUAMSC sheets are equivalent to that of human saphenous veins [30], suggesting that our hUASMC grafts were strong enough to withstand arterial blood pressure.
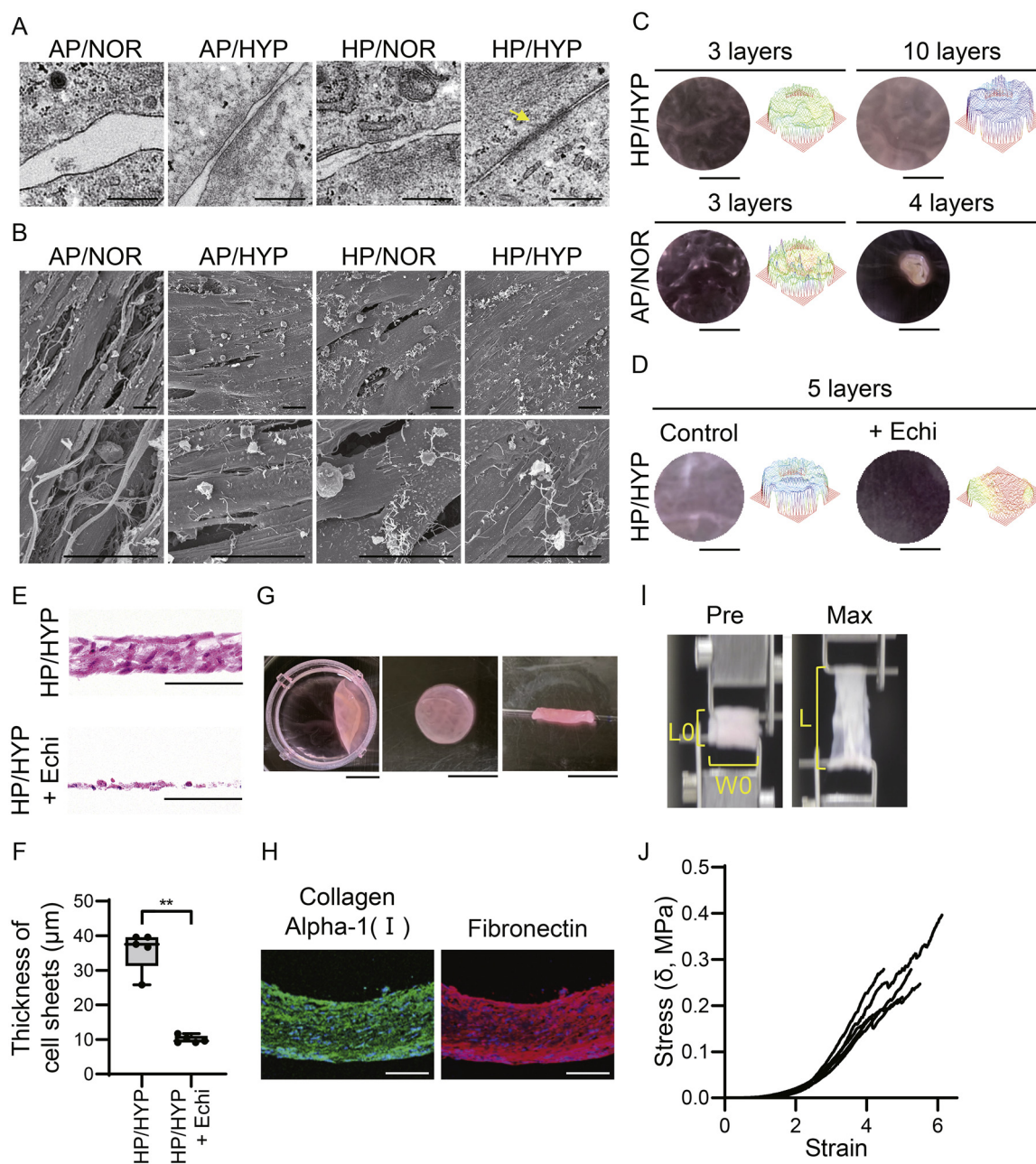
Fig. 4. Layered constructs of hUASMCs generated by repeated cell seeding and HP/HYP culture. (A) Representative images of transmission electron microscopy of 3-layered hUASMC sheets fabricated with AP/NOR, AP/HYP, HP/NOR, or HP/HYP. Adherence junctions are indicated by arrows. Scale bars: 500 nm. (B) Representative images of scanning electron microscopy of 3-layered hUASMC sheets fabricated with AP/NOR, AP/HYP, HP/NOR, or HP/HYP. Upper and lower images are low ($\times$ 500) and high ($\times$ 2000) power field, respectively. Scale bars: 20 μm. (C) Representative macroscopic (left) and surface plot images (right) of hUASMC sheets fabricated with AP/NOR or HP/HYP. Scale bars: 5 mm. (D) Representative macroscopic (left) and surface plot images (right) of 5-layered hUASMC sheets fabricated by HP/HYP treated with or without echinomycin (Echi). Scale bars: 5 mm. (E) Representative hematoxylin and eosin stain images of 5-layered hUASMC sheets fabricated by HP/HYP with or without echinomycin. Scale bars: 50 μm. (F) Quantification of the thickness of (E); $n = 5$. $^{**}P < 0.01$. Boxes represent the medians and interquartile range; whiskers indicate the minimum to maximum values. (G) Representative images of a 10-layered hUASMC sheet by cell seeding and HP/HYP on an atelocollagen membrane (left). The cell sheet after detachment (middle) was wrapped around a glass mandrel to fabricate a tubular hUASMC graft (right). Scale bars: 10 mm. (H) Representative images of immunocytochemistry of 10-layered hUASMC grafts. Grafts were stained for collagen alpha-1(I) (green) and fibronectin (red). Scale bars: 100 μm. (I) Representative images of mechanical testing of an hUASMC graft. A tubular hUASMC graft was placed around two parallel hooks of stainless-steel wire. An hUASMC graft before pulling (Pre) and a maximum stretched hUASMC sheet (Max). W0 and L0 indicate the initial sample width and sample length, respectively; L indicates sample length during the pulling. (J) Stress-strain behaviors of each hUASMC graft; $n = 5$. (For interpretation of the references to color in this figure legend, the reader is referred to the web version of this article.)

3.6. Implantation of human VSMC grafts in the rat aorta and remodeling of the implanted site of the vessel

Patch grafts are used for reconstruction of the pulmonary artery and aorta in pediatric patients with congenital heart disease [31] and for endarterectomy repair of the femoral and carotid artery in adult patients [32]. We implanted hUASMC and ePTFE grafts in the rat abdominal aorta with the intention of applying patch autografts to pediatric and adult patients. An hUASMC or ePTFE graft trimmed to 1.5 $\times$ 1.0 mm as a patch graft was sutured in an adult nude rat abdominal aorta with a 1.5-mm longitudinal incision (Fig. 5A and S7A and B). Doppler echocardiogra-
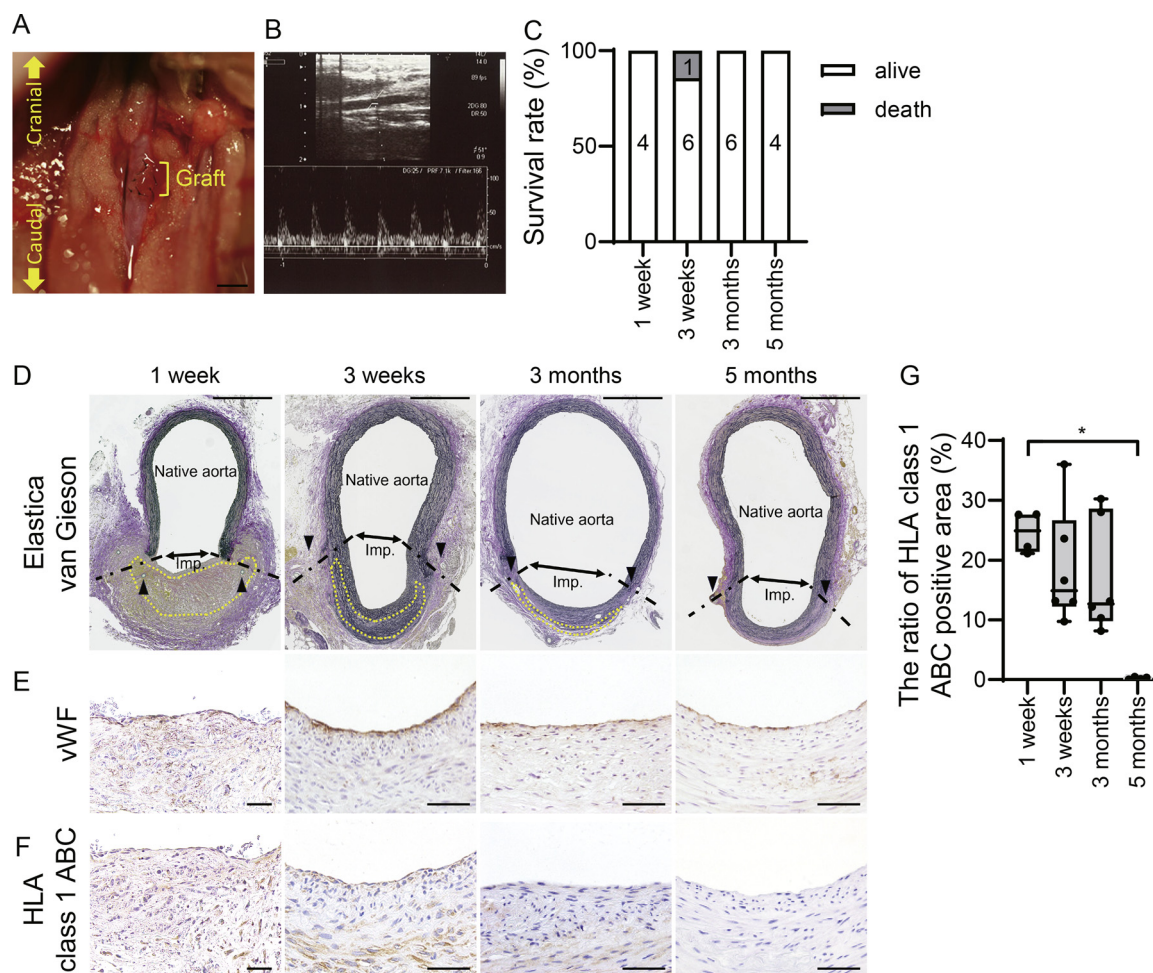
Fig. 5. Implantation of hUASMC grafts in the rat abdominal aorta. (A) Representative macroscopic image of the rat aorta after implantation of an hUASMC graft. Scale bar: 1 mm. (B) Doppler echocardiography detected a non-stenotic flow pattern below the implantation site 5 months after implantation. (C) Survival rate of rats 1 week ($n = 4$), 3 weeks ($n = 7$), 3 months ($n = 6$), and 5 months ($n = 4$) after implantation. (D) Elastica van Gieson stain images of the rat abdominal aorta implanted with hUASMC grafts 1 week, 3 weeks, 3 months, and 5 months after implantation. The dotted lines indicate a junction between the hUASMC graft and the native aorta. The yellow dotted lines indicate implanted hUASMCs. The arrowheads indicate a suture line. Imp.: implantation site. Scale bars: 500 μm. (E and F) Representative images of immunohistochemistry of vWF (von Willebrand factor) (E) and HLA class 1 ABC (F) at the implantation sites. Scale bars: 50 μm. (G) Semiquantitative analysis of (F). $n = 4$–6. *$P < 0.05$. Boxes represent the medians and interquartile range; whiskers indicate the minimum to maximum values. (For interpretation of the references to color in this figure legend, the reader is referred to the web version of this article.)

phy detected a non-stenotic flow pattern distal to the implantation site of hUASMC grafts, and a pulsatile implantation site was observed macroscopically 5 months after implantation (Fig. 5B and Movie S2). During the observation until dissection, one rat implanted with an hUASMC graft and one rat implanted with an ePTFE graft died several days after implantation due to suture failure; however, 20 of 21 rats implanted with hUASMC grafts and 5 of 6 rats implanted with ePTFE grafts remained alive (Fig. 5C).

Histological analysis of implantation sites with hUASMC grafts demonstrated the absence of aneurysm formation at the implantation site through 5 months after implantation, and von Willebrand factor-positive endothelial cells completely covered the luminal side of implanted hUASMC graft 1 week after implantation (Fig. 5D and E). HLA class 1 ABC-positive human-derived cells remained until 3 months after implantation and then gradually decreased. Implanted hUASMCs had disappeared completely 5 months after implantation (Fig. 5F and G). hUASMC grafts attached firmly to the surrounding tissues, whereas ePTFE grafts were easily detached from surrounding tissues during dissection (Fig. S7C), as reported previously [33]. These data suggested that recipient-derived cells migrated into the hUASMC graft-derived ECM structure and replaced implanted hUASMCs. In addition, a substantial number of

CD45-positive leukocytes was detected in tissues surrounding the ePTFE graft, whereas modest leukocyte infiltration was observed at the implantation site of the hUASMC graft (Fig. S7D and E).

We then tried implantation of larger grafts. hUASMC grafts trimmed to 4.0 × 1.0 mm were implanted in a rat abdominal aorta with a 4.0-mm longitudinal incision (Fig. S8A). Although hUASMC grafts withstood arterial blood pressure immediately after transplantation ($n = 4$), implantation sites exhibited aneurysmal formation 1 week after implantation (Fig. S8B), suggesting that larger hUASMC grafts need to be improved to withstand blood pressure.

Finally, we investigated elastic fiber formation, collagen production, and SMC phenotypes at the site of implantation of hUASMC grafts. Fewer elastic fibers were observed in hUASMC grafts than in the native aorta before implantation; however, modest formation of elastic fibers was observed at the implantation site 3 weeks after implantation compared to the native rat aorta and gradually increased over time. Elastic fiber content at the implantation site approached that of the aorta 5 months after implantation (Fig. 6A and B). Sirius red stain showed that the implanted sites had a comparable amount of collagen to that of the aorta at least up to 5 months after implantation (Fig. 6C and D). The ratio of collagen type I and type III and the protein expression levels of the ma-
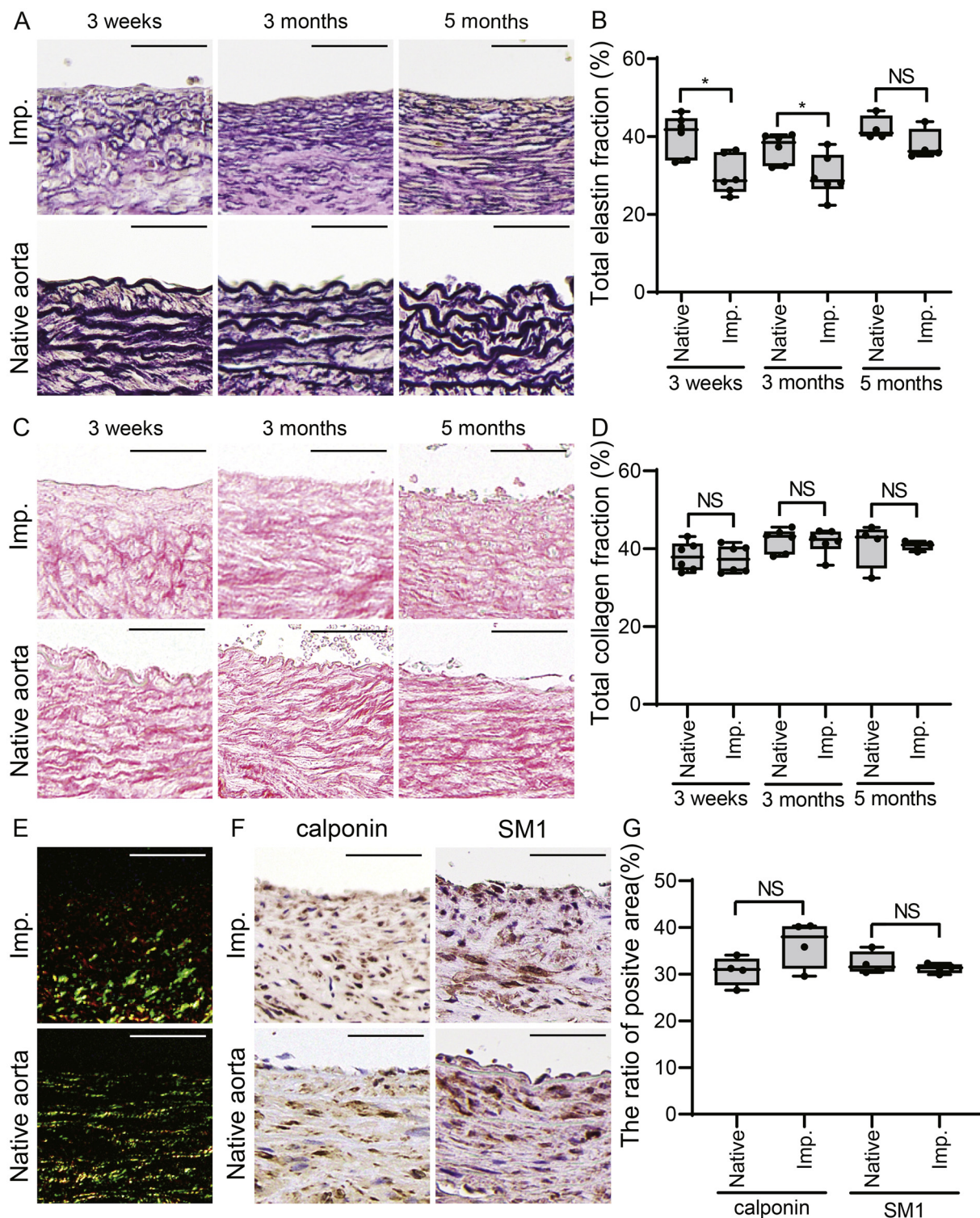
Fig. 6. Extracellular matrix deposition and smooth muscle cell phenotype 3 weeks, 3 months, and 5 months after implantation of hUASMC grafts. (A) Representative images of Elastica van Gieson stain at the implantation sites (Imp.) and native rat aortas 3 weeks, 3 months, and 5 months after implantation. Scale bars: 50 μm. (B) Semiquantitative analysis of (A). Native: native aorta; Imp: implantation site; $n = 4$–6. (C) Representative images of picrosirius red stain at the implantation sites and native rat aortas 3 weeks, 3 months, and 5 months after implantation. Scale bars: 50 μm. (D) Semiquantitative analysis of (C); $n = 4$–6. (E) Representative images of picrosirius red stain under polarized light at the implantation site and native rat aorta 5 months after implantation. Orange and green colors indicate collagen I and III, respectively. Scale bars: 50 μm. (F) Representative images of immunohistochemistry of calponin and SM1 at the implantation site and native rat aorta 5 months after implantation. Scale bars: 50 μm. (G) Semiquantitative analysis of (F); $n = 4$. NS, not significant, $*P < 0.05$. Boxes represent the medians and interquartile range; whiskers indicate the minimum to maximum values. (For interpretation of the references to color in this figure legend, the reader is referred to the web version of this article.)

ture VSMC markers calponin and SM1 were similar between the implantation sites and native aorta 5 months after implantation (Fig. 6E–G).

4. Discussion

In this study, we showed that hydrostatic pressurization combined with a hypoxic environment enabled the 3-dimensional fabrication of multi-layered tunica media derived from human VSMCs, which contained N-cadherin-mediated cell-cell adhesions, cell-ECM junctions via clustering of integrin $\alpha5\beta1$, and fibronectin and collagen fibrillogenesis. The scaffoldless VSMC grafts fabricated by repeated cell seeding and HP/HYP culture had high biocompatibility and induced regeneration of the vessels.

In cancer cells, NDRG1 promotes formation of an E-cadherin/β-catenin complex at the cell membrane and strengthens cell-cell adhesions, which acts as a suppressor of metastasis [23]. To the best of our knowledge, we first demonstrated that NDRG1 played a primary role in N-cadherin-mediated cell-cell adhesion. The *NDRG1* gene contains hypoxia-responsive elements (HRE), and HIF-1α plays a role in regulating hypoxia-induced *NDRG1* transcription [34]. In addition, various transcription factors for the regulation of *NDRG1* expression have been reported [35]. In the present study, C/EBPα appeared to be involved in *NDRG1* upregulation but HIF-1α did not, although HP/HYP did not change the expression of C/EBPα in the nuclear fraction compared with AP/HYP (Fig. S9). Our results showed that HIF-1α expression was markedly enhanced by dual treatments of mechanical loading and hypoxia compared with the individual treatment, which is similar to findings in a previous study [36]. It has been reported that the transcriptional activity of C/EBPα is enhanced under transfection of both C/EBPα and HIF-1α compared with that of C/EBPα or HIF-1α alone in COS7 and 293T cell lines [37]. The transactivation domain of C/EBPα directly interacts with the basic helix-loop-helix domain of HIF-1α [38]. In addition, mechanical loading increases the DNA-binding activity of C/EBPα in human airway smooth muscle cells [39]. Based on these findings, we speculated that mechanical loading-mediated enhancement of HIF-1α expression increased the transcriptional activity of C/EBPα, resulting in *NDRG1* upregulation. Contrary to this expectation, our results showed that silencing of *HIF1A* did not affect HP/HYP-induced NDRG1 upregulation. Although the mechanism of the complicated interaction between HIF-1α and C/EBPα under HP/HYP culture conditions is unknown, C/EBPα might be important for the regulation of NDRG1 transcription levels in hUASMCs independently from HIF-1α.

Integrin receptors play a role in the transmembrane link between ECMs and actin cytoskeleton in VSMCs [40]. Integrin $\alpha5\beta1$ is the major receptor for fibronectin, which is an indispensable factor for the initiation of ECM assemblies [41]. Global deletion of integrin $\alpha5$ subunit or fibronectin in mice leads to embryonic lethality, with severe abnormalities of the heart and blood vessels [42,43]. Hence, the interaction of integrin $\alpha5\beta1$ and fibronectin is necessary for blood vessel development. Fibronectin binding further stabilizes and activates integrin clustering [44,45]. In the tissue engineering field, Pezzoli et al. reported that cellularized TEVGs supplemented with human plasma fibronectin enhanced mechanical strength [46]. These data suggest that HP/HYP-induced clustering of integrin $\alpha5\beta1$ and fibronectin fibrillogenesis contributed to the high mechanical strength of the grafts derived from hUASMCs.

LOX is an essential enzyme for initiating cross-link formation in collagen fibrils [27] and ordered collagen fibrinogenesis [28]. Inactivation of LOX causes a decline in the tensile strength of the arterial walls; thus, LOX is important for the mechanical development of large arterial walls [47]. In addition, LOX-mediated ECM cross-linking increases mechanical strength in TEVGs using LOX-

overexpression VSMCs [48]. These findings indicate that the promotion of collagen cross-linking by HP/HYP-induced LOX expression is advantageous for making high-strength grafts. A recent report showed that EMILIN1 (elastin-microfibril-interface-located-protein-1) is involved in LOX-mediated collagen cross-linking [49]. Collagen type V is reportedly essential for the assembly of collagen fibrils [50]. In our RNA-sequencing data, both *EMILIN1* and *COL5A1* were upregulated in HP/HYP culture (Table S4). EMILIN1 and collagen type V, together with LOX, may contribute to collagen fibril formation in our grafts.

4-Hydroxyproline, which is enzymatically modified by collagen prolyl 4-hydroxylases (P4H) from proline within collagen polypeptides sequences, is essential for the thermal stability of collagens at body temperature [51]. Gilkes et al. demonstrated that HIF-1α-induced expression of P4HA1 and P4HA2, the catalytic subunits of P4H, was required for collagen deposition in fibroblasts [52]. In addition, Aro et al. demonstrated that HIF-1α-induced mRNA expression of *P4HA1* and *P4HA2* led to increasing prolyl hydroxylase activity, which was necessary for collagen synthesis in chondrocytes in a hypoxic environment [53]. Hence, HIF-1α-induced P4HA1 and P4HA2 expression and subsequent increase in prolyl hydroxylase activity are required for proper collagen synthesis and assembly. In our RNA-sequencing data, expression of *P4HA1* and *P4HA2* was most increased by HP/HYP compared with the other culture conditions (Table S6), and these expression patterns were similar to that of HIF-1α. These findings indicated that HP/HYP-induced *P4HA1* and *P4HA2* expression increased the activity of prolyl hydroxylase, which may contribute to collagen synthesis in hUASMC grafts.

Five months after implantation of our VSMCs grafts, the transplantation site was composed of recipient-derived VSMCs exhibiting a contractile phenotype and regenerated elastin laminae. The development of TEVGs that promote the regeneration of adequate elastin laminae has long been a challenge [54,55]. Recently, Wang et al. fabricated a biodegradable vascular graft with human recombinant tropoelastin embedded within a polyglycerol sebacate scaffold using the electrospinning method [56]. This graft showed long-term patency and promoted the regeneration of multiple elastic lamellae and internal elastic lamina. However, we were concerned that several properties of elastin fibrils (high thrombogenicity and inhibiting VSMCs proliferation) might limit the clinical application of the elastic fiber–rich TEVGs [56,57]. Although liquid chromatography-tandem mass spectrometry (LC-MS/MS) analyses demonstrated the presence of desmosine and isodesmosine, Elastica van Gieson stain failed to detect elastic lamella structures in our hUASMC grafts at implantation, suggesting that the hUASMC grafts included cross-linking elastic fibers but in a small amount. In the present study, elastic lamellae were induced after replacement of the implanted hUASMCs with host-derived cells. The induction of elastic lamellae after implantation may be a favorable strategy to avoid these concerns.

To prevent graft rejection, autologous cell sources with high proliferative capacity and ECM production are needed for the fabrication of TEVGs. hUASMCs exhibit greater ECM secretion and carry no risk of carcinogenesis, and there are no ethical issues with their use [58]. Therefore, human umbilical arteries could be an ideal cell source for pediatric patients with congenital heart disease. In adults, several clinical trials using autologous TEVGs derived from the patient's own fibroblasts for hemodialysis access have been conducted [15,59]. Our results showed that HP/HYP treatment upregulated *NDRG1* and *LOX* expression in fibroblasts to the same degree as that of hUASMCs. These results support the feasibility of HP/HYP-treated fibroblasts as a cell source for autologous TEVGs. Further studies are needed to clarify the availability of HP/HYP-induced fabrication of vascular grafts using fibroblasts.

In pediatric patients with congenital heart disease, reconstruction of large vessels using patch grafts is a common surgical

technique [31]. In adult patients with atherosclerosis, patch grafts are commonly used for arteriotomy closure following femoral and carotid endarterectomy [32]. In the present study, we aimed to investigate whether 1.5 × 1.0 mm patch grafts without endothelial cells were biocompatible and found that the grafts were covered with the recipient-derived cells and became endothelialized 1 week after implantation. The method proposed in this study has the theoretical potential to fabricate vascular grafts containing endothelial cells. However, the graft size (1.5 × 1.0 mm) was smaller than that reported by other laboratories [60–63]. We attempted implantation using 4.0 × 1.0 mm patch grafts; implantation was successful but exhibited aneurysmal dilation 1 week after the implantation period. Tubular grafts are also widely used in adult patients for coronary arterial bypass and hemodialysis access. In our previous study, implanted tubular grafts made from multi-layered rat VSMC constructs were obstructed due to intraluminal thrombosis within 2.5 months [17]. For small-caliber tubular grafts, endothelial cells are thought to be required to decrease thrombogenicity [15,59]. Further improvement of the fabrication method (i.e., endothelial coverage) will be needed to fabricate large patch grafts and tubular grafts.

The 10-layered VSMC grafts fabricated in this study required 34 days. A long culture period results in high medical costs and delayed surgical schedules. Various procedures have recently been developed for fabricating scaffold-based or scaffoldless TEVGs [64]. The Kenzan method of 3-dimensional bioprinting enabled fabrication of scaffoldless TEVGs within 1 month [65]. The decellularization method could provide "off-the-shelf" arterial grafts without the need for ECM maturation periods [66]. Thus, further improvement of the protocols to shorten fabrication time will be needed for clinical application.

Ideal animal models for evaluating the performance of TEVGs should have similar cardiovascular anatomy and physiology to humans. Rats are the most commonly used animal model due to the advantages of low cost and availability of genetically modified strains. However, cardiovascular physiology, thrombogenicity, and hemostasis mechanisms in rats are different from those in humans [67,68] and large animals such as sheep, pigs, and non-human primates. Commercialized scaffoldless TEVGs by Cytograft Tissue Engineering Inc., which have already been used clinically for hemodialysis access [64], were used in preclinical trials using non-human primates. This preclinical trial confirmed the absence of aneurysmal formation, which is a common complication of TEVG implantation [14]. For the challenge of clinical application of our scaffoldless VSMCs grafts, further in vivo studies using large animals are needed to confirm the absence of complications such as aneurysmal formation.

In conclusion, our results suggest that HP/HYP culture can be used to fabricate high-strength, scaffoldless implantable human VSMC grafts through increased cell-cell and cell-ECM adhesion; moreover, HP/HYP culture has the ability to build robust ECM networks.

Declaration of Competing Interest

The authors declare that they have no known competing financial interests or personal relationships that could have appeared to influence the work reported in this paper.

CRediT authorship contribution statement

Tomoyuki Kojima: Conceptualization, Formal analysis, Investigation, Data curation, Writing – original draft, Visualization. **Takashi Nakamura:** Validation, Formal analysis, Investigation, Data curation, Writing – original draft, Visualization, Funding acquisition. **Junichi Saito:** Conceptualization, Investigation, Funding ac-

quisition. **Yuko Hidaka:** Investigation, Investigation. **Taisuke Akimoto:** Investigation. **Hana Inoue:** Investigation. **Christian Nanga Chick:** Investigation. **Toyonobu Usuki:** Resources, Writing – review & editing. **Makoto Kaneko:** Resources, Writing – review & editing, Funding acquisition. **Etsuko Miyagi:** Resources, Writing – review & editing. **Yoshihiro Ishikawa:** Writing – review & editing. **Utako Yokoyama:** Conceptualization, Methodology, Writing – review & editing, Supervision, Project administration, Funding acquisition.

Supplementary materials

Supplementary material associated with this article can be found, in the online version, at doi:10.1016/j.actbio.2023.09.041.

References

[1] S.S. Virani, A. Alonso, E.J. Benjamin, M.S. Bittencourt, C.W. Callaway, A.P. Carson, A.M. Chamberlain, A.R. Chang, S. Cheng, F.N. Delling, L. Djousse, M.S.V. Elkind, J.F. Ferguson, M. Fornage, S.S. Khan, B.M. Kissela, K.L. Knutson, T.W. Kwan, D.T. Lackland, T.T. Lewis, J.H. Lichtman, C.T. Longenecker, M.S. Loop, P.L. Lutsey, S.S. Martin, K. Matsushita, A.E. Moran, M.E. Mussolino, A.M. Perak, W.D. Rosamond, G.A. Roth, U.K.A. Sampson, G.M. Satou, E.B. Schroeder, S.H. Shah, C.M. Shay, N.L. Spartano, A. Stokes, D.L. Tirschwell, L.B. VanWagner, C.W. Tsao, Heart disease and stroke statistics-2020 update: a report from the American heart association, Circulation 141 (9) (2020) e139–e596.
[2] D. van der Linde, E.E. Konings, M.A. Slager, M. Witsenburg, W.A. Helbing, J.J. Takkenberg, J.W. Roos-Hesselink, Birth prevalence of congenital heart disease worldwide: a systematic review and meta-analysis, J. Am. Coll. Cardiol. 58 (21) (2011) 2241–2247.
[3] D.P. Taggart, Current status of arterial grafts for coronary artery bypass grafting, Ann. Cardiothorac. Surg. 2 (4) (2013) 427–430.
[4] A.Y. Lee, N. Mahler, C. Best, Y.U. Lee, C.K. Breuer, Regenerative implants for cardiovascular tissue engineering, Transl. Res. J. Lab. Clin. Med. 163 (4) (2014) 321–341.
[5] D.A.C. Walma, K.M. Yamada, The extracellular matrix in development, Development 147 (10) (2020) dev175596.
[6] K.A. Athanasiou, R. Eswaramoorthy, P. Hadidi, J.C. Hu, Self-organization and the self-assembling process in tissue engineering, Annu. Rev. Biomed. Eng. 15 (2013) 115–136.
[7] J. Saito, M. Kaneko, Y. Ishikawa, U. Yokoyama, Challenges and possibilities of cell-based tissue-engineered vascular grafts, Cyborg Bionic Syst. 2021 (2021) 1532103.
[8] S. Fang, D.G. Ellman, D.C. Andersen, Review: tissue engineering of small-diameter vascular grafts and their in vivo evaluation in large animals and humans, Cells 10 (3) (2021) 713.
[9] Y. Torres, M. Gluais, N. Da Silva, S. Rey, A. Grémare, L. Magnan, F. Kawecki, N. L'Heureux, Cell-assembled extracellular matrix (CAM) sheet production: translation from using human to large animal cells, J. Tissue Eng. 12 (2021) 2041731420978327.
[10] R. Iwaki, T. Shoji, Y. Matsuzaki, A. Ulziibayar, T. Shinoka, Current status of developing tissue engineering vascular technologies, Expert Opin. Biol. Ther. 22 (3) (2022) 433–440.
[11] M.C. Simon, B. Keith, The role of oxygen availability in embryonic development and stem cell function, Nat. Rev. Mol. Cell Biol. 9 (4) (2008) 285–296.
[12] J.E. Wagenseil, R.P. Mecham, Vascular extracellular matrix and arterial mechanics, Physiol. Rev. 89 (3) (2009) 957–989.
[13] N. L'Heureux, S. Pâquet, R. Labbé, L. Germain, F.A. Auger, A completely biological tissue-engineered human blood vessel, Faseb J. 12 (1) (1998) 47–56.
[14] N. L'Heureux, N. Dusserre, G. Konig, B. Victor, P. Keire, T.N. Wight, N.A. Chronos, A.E. Kyles, C.R. Gregory, G. Hoyt, R.C. Robbins, T.N. McAllister, Human tissue-engineered blood vessels for adult arterial revascularization, Nat. Med. 12 (3) (2006) 361–365.
[15] T.N. McAllister, M. Maruszewski, S.A. Garrido, W. Wystrychowski, N. Dusserre, A. Marini, K. Zagalski, A. Fiorillo, H. Avila, X. Manglano, J. Antonelli, A. Kocher, M. Zembala, L. Cierpka, L.M. de la Fuente, N. L'Heureux, Effectiveness of haemodialysis access with an autologous tissue-engineered vascular graft: a multicentre cohort study, Lancet 373 (9673) (2009) 1440–1446.

[16] J. Saito, U. Yokoyama, T. Nakamura, T. Kanaya, T. Ueno, Y. Naito, T. Takayama, M. Kaneko, S. Miyagawa, Y. Sawa, Y. Ishikawa, Scaffold-free tissue-engineered arterial grafts derived from human skeletal myoblasts, Artif. Organs 45 (8) (2021) 919–932.

[17] U. Yokoyama, Y. Tonooka, R. Koretake, T. Akimoto, Y. Gonda, J. Saito, M. Umemura, T. Fujita, S. Sakuma, F. Arai, M. Kaneko, Y. Ishikawa, Arterial graft with elastic layer structure grown from cells, Sci. Rep. 7 (1) (2017) 140.

[18] S.R. Mohapatra, E. Rama, C. Melcher, T. Call, M.A. Al Enezy-Ulbrich, A. Pich, C. Apel, F. Kiessling, S. Jockenhoevel, From in vitro to perioperative vascular tissue engineering: shortening production time by traceable textile-reinforcement, Tissue Eng. Regen. Med. 19 (6) (2022) 1169–1184.

[19] M. Rafique, T. Wei, Q. Sun, A.C. Midgley, Z. Huang, T. Wang, M. Shafiq, D. Zhi, J. Si, H. Yan, D. Kong, K. Wang, The effect of hypoxia-mimicking responses on improving the regeneration of artificial vascular grafts, Biomaterials 271 (2021) 120746.

[20] J. Guo, J. Huang, S. Lei, D. Wan, B. Liang, H. Yan, Y. Liu, Y. Feng, S. Yang, J. He, D. Kong, J. Shi, S. Wang, Construction of rapid extracellular matrix-deposited small-diameter vascular grafts induced by hypoxia in a bioreactor, ACS Biomater. Sci. Eng. 9 (2) (2023) 844–855.

[21] A. Subramanian, P. Tamayo, V.K. Mootha, S. Mukherjee, B.L. Ebert, M.A. Gillette, A. Paulovich, S.L. Pomeroy, T.R. Golub, E.S. Lander, J.P. Mesirov, Gene set enrichment analysis: a knowledge-based approach for interpreting genome-wide expression profiles, Proc. Natl. Acad. Sci. U.S.A. 102 (43) (2005) 15545–15550.

[22] Z. Sun, A.R. Parrish, M.A. Hill, G.A. Meininger, N-cadherin, a vascular smooth muscle cell-cell adhesion molecule: function and signaling for vasomotor control, Microcirculation 21 (3) (2014) 208–218.

[23] J. Sun, D. Zhang, D.H. Bae, S. Sahni, P. Jansson, Y. Zheng, Q. Zhao, F. Yue, M. Zheng, Z. Kovacevic, D.R. Richardson, Metastasis suppressor, NDRG1, mediates its activity through signaling pathways and molecular motors, Carcinogenesis 34 (9) (2013) 1943–1954.

[24] Q. Wang, L.H. Li, G.D. Gao, G. Wang, L. Qu, J.G. Li, C.M. Wang, HIF-1α up-regulates NDRG1 expression through binding to NDRG1 promoter, leading to proliferation of lung cancer A549 cells, Mol. Biol. Rep. 40 (5) (2013) 3723–3729.

[25] J. Yamaguchi, T. Tanaka, H. Saito, S. Nomura, H. Aburatani, H. Waki, T. Kadowaki, M. Nangaku, Echinomycin inhibits adipogenesis in 3T3-L1 cells in a HIF-independent manner, Sci. Rep. 7 (1) (2017) 6516.

[26] M.A. Glukhova, J.P. Thiery, Fibronectin and integrins in development, Semin. Cancer Biol. 4 (4) (1993) 241–249.

[27] H.M. Kagan, W. Li, Lysyl oxidase: properties, specificity, and biological roles inside and outside of the cell, J. Cell. Biochem. 88 (4) (2003) 660–672.

[28] A. Herchenhan, F. Uhlenbrock, P. Eliasson, M. Weis, D. Eyre, K.E. Kadler, S.P. Magnusson, M. Kjaer, Lysyl oxidase activity is required for ordered collagen fibrillogenesis by tendon cells, J. Biol. Chem. 290 (26) (2015) 16440–16450.

[29] J. Thomas, D.F. Elsden, S.M. Partridge, Partial structure of two major degradation products from the cross-linkages in elastin, Nature 200 (1963) 651–652.

[30] G. Konig, T.N. McAllister, N. Dusserre, S.A. Garrido, C. Iyican, A. Marini, A. Fiorillo, H. Avila, W. Wystrychowski, K. Zagalski, M. Maruszewski, A.L. Jones, L. Cierpka, L.M. de la Fuente, N. L'Heureux, Mechanical properties of completely autologous human tissue engineered blood vessels compared to human saphenous vein and mammary artery, Biomaterials 30 (8) (2009) 1542–1550.

[31] V.H.M. Weixler, K. Kuschnerus, O. Romanchenko, S. Ovroutski, M.Y. Cho, F. Berger, M. Sigler, N. Sinzobahamvya, J. Photiadis, P. Murin, Mid-term performance of decellularized equine pericardium in congenital heart surgery, Interact. Cardiovasc. Thorac. Surg. 36 (2022) ivac269.

[32] K.B. Allen, J.D. Adams, S.F. Badylak, H.E. Garrett, N.J. Mouawad, S.W. Oweida, M. Parikshak, P.K. Sultan, Extracellular matrix patches for endarterectomy repair, Front. Cardiovasc. Med. 8 (2021) 631750.

[33] K. Shimada, A. Higuchi, R. Kubo, T. Murakami, Y. Nakazawa, R. Tanaka, The effect of a silk Fibroin/Polyurethane blend patch on rat Vessels, Organogenesis 13 (4) (2017) 115–124.

[34] A. Kitowska, T. Pawełczyk, N-myc downstream regulated 1 gene and its place in the cellular machinery, Acta Biochim. Pol. 57 (1) (2010) 15–21.

[35] H.M. Said, R. Safari, G. Al-Kafaji, R.I. Ernestus, M. Löhr, A. Katzer, M. Flentje, C. Hagemann, Time- and oxygen-dependent expression and regulation of NDRG1 in human brain cancer cells, Oncol. Rep. 37 (6) (2017) 3625–3634.

[36] S. Shimomura, H. Inoue, Y. Arai, S. Nakagawa, Y. Fujii, T. Kishida, M. Shin-Ya, S. Ichimaru, S. Tsuchida, O. Mazda, K. Takahashi, Mechanical stimulation of chondrocytes regulates HIF-1α under hypoxic conditions, Tissue Cell 71 (2021) 101574.

[37] Y. Jiang, Z.H. Xue, W.Z. Shen, K.M. Du, H. Yan, Y. Yu, Z.G. Peng, M.G. Song, J.H. Tong, Z. Chen, Y. Huang, M. Lübbert, G.Q. Chen, Desferrioxamine induces leukemic cell differentiation potentially by hypoxia-inducible factor-1 alpha that augments transcriptional activity of CCAAT/enhancer-binding protein-alpha, Leukemia 19 (7) (2005) 1239–1247.

[38] L. Yang, Y. Jiang, S.F. Wu, M.Y. Zhou, Y.L. Wu, G.Q. Chen, CCAAT/enhancer-binding protein alpha antagonizes transcriptional activity of hypoxia-inducible factor 1 alpha with direct protein-protein interaction, Carcinogenesis 29 (2) (2008) 291–298.

[39] A. Kumar, A.J. Knox, A.M. Boriek, CCAAT/enhancer-binding protein and activator protein-1 transcription factors regulate the expression of interleukin-8 through the mitogen-activated protein kinase pathways in response to mechanical stretch of human airway smooth muscle cells, J. Biol. Chem. 278 (21) (2003) 18868–18876.

[40] E.P. Moiseeva, Adhesion receptors of vascular smooth muscle cells and their functions, Cardiovasc. Res. 52 (3) (2001) 372–386.

[41] H. Kumra, D.P. Reinhardt, Fibronectin-targeted drug delivery in cancer, Adv. Drug Deliv. Rev. 97 (2016) 101–110.

[42] S.E. Francis, K.L. Goh, K. Hodivala-Dilke, B.L. Bader, M. Stark, D. Davidson, R.O. Hynes, Central roles of alpha5beta1 integrin and fibronectin in vascular development in mouse embryos and embryoid bodies, Arterioscler. Thromb. Vasc. Biol. 22 (6) (2002) 927–933.

[43] E.L. George, H.S. Baldwin, R.O. Hynes, Fibronectins are essential for heart and blood vessel morphogenesis but are dispensable for initial specification of precursor cells, Blood 90 (8) (1997) 3073–3081.

[44] D. Jülich, G. Cobb, A.M. Melo, P. McMillen, A.K. Lawton, S.G. Mochrie, E. Rhoades, S.A. Holley, Cross-scale integrin regulation organizes ECM and tissue topology, Dev. Cell 34 (1) (2015) 33–44.

[45] G. Sun, E. Guillon, S.A. Holley, Integrin intra-heterodimer affinity inversely correlates with integrin activatability, Cell Rep. 35 (10) (2021) 109230.

[46] D. Pezzoli, J. Di Paolo, H. Kumra, G. Fois, G. Candiani, D.P. Reinhardt, D. Mantovani, Fibronectin promotes elastin deposition, elasticity and mechanical strength in cellularised collagen-based scaffolds, Biomaterials 180 (2018) 130–142.

[47] J.M. Mäki, J. Räsänen, H. Tikkanen, R. Sormunen, K. Mäkikallio, K.I. Kivirikko, R. Soininen, Inactivation of the lysyl oxidase gene Lox leads to aortic aneurysms, cardiovascular dysfunction, and perinatal death in mice, Circulation 106 (19) (2002) 2503–2509.

[48] W.M. Elbjeirami, E.O. Yonter, B.C. Starcher, J.L. West, Enhancing mechanical properties of tissue-engineered constructs via lysyl oxidase crosslinking activity, J. Biomed. Mater. Res. A 66 (3) (2003) 513–521.

[49] C.S. Adamo, A. Beyens, A. Schiavinato, D.R. Keene, S.F. Tufa, M. Mörgelin, J. Brinckmann, T. Sasaki, A. Niehoff, M. Dreiner, L. Pottie, L. Muiño-Mosquera, E.Y. Gulec, A. Gezdirici, P. Braghetta, P. Bonaldo, R. Wagener, M. Paulsson, H. Bornaun, R. De Rycke, M. De Bruyne, F. Baeke, W.P. Devine, B. Gangaram, A. Tam, M. Balasubramanian, S. Ellard, S. Moore, S. Symoens, J. Shen, S. Cole, U. Schwarze, K.W. Holmes, S.J. Hayflick, W. Wiszniewski, S. Nampoothiri, E.C. Davis, L.Y. Sakai, G. Sengle, B. Callewaert, EMILIN1 deficiency causes arterial tortuosity with osteopenia and connects impaired elastogenesis with defective collagen fibrillogenesis, Am. J. Hum. Genet. 109 (12) (2022) 2230–2252.

[50] R.J. Wenstrup, J.B. Florer, E.W. Brunskill, S.M. Bell, I. Chervoneva, D.E. Birk, Type V collagen controls the initiation of collagen fibril assembly, J. Biol. Chem. 279 (51) (2004) 53331–53337.

[51] P. Ratcliffe, P. Koivunen, J. Myllyharju, J. Ragoussis, J.V. Bovée, I. Batinic-Haberle, C. Vinatier, V. Trichet, F. Robriquet, L. Oliver, B. Gardie, Update on hypoxia-inducible factors and hydroxylases in oxygen regulatory pathways: from physiology to therapeutics, Hypoxia (Auckl) 5 (2017) 11–20.

[52] D.M. Gilkes, S. Bajpai, P. Chaturvedi, D. Wirtz, G.L. Semenza, Hypoxia-inducible factor 1 (HIF-1) promotes extracellular matrix remodeling under hypoxic conditions by inducing P4HA1, P4HA2, and PLOD2 expression in fibroblasts, J. Biol. Chem. 288 (15) (2013) 10819–10829.

[53] E. Aro, R. Khatri, R. Gerard-O'Riley, L. Mangiavini, J. Myllyharju, E. Schipani, Hypoxia-inducible factor-1 (HIF-1) but not HIF-2 is essential for hypoxic induction of collagen prolyl 4-hydroxylases in primary newborn mouse epiphyseal growth plate chondrocytes, J. Biol. Chem. 287 (44) (2012) 37134–37144.

[54] J. Fu, X. Ding, C.E.T. Stowell, Y.L. Wu, Y. Wang, Slow degrading poly(glycerol sebacate) derivatives improve vascular graft remodeling in a rat carotid artery interposition model, Biomaterials 257 (2020) 120251.

[55] J. Fu, M. Wang, I. De Vlaminck, Y. Wang, Thick PCL fibers improving host remodeling of PGS-PCL composite grafts implanted in rat common carotid arteries, Small 16 (52) (2020) e2004133.

[56] Z. Wang, S.M. Mithieux, H. Vindin, Y. Wang, M. Zhang, L. Liu, J. Zbinden, K.M. Blum, T. Yi, Y. Matsuzaki, F. Oveissi, R. Akdemir, K.M. Lockley, L. Zhang, K. Ma, J. Guan, A. Waterhouse, N.T.H. Pham, B.S. Hawkett, T. Shinoka, C.K. Breuer, A.S. Weiss, Rapid regeneration of a neoartery with elastic lamellae, Adv. Mater. 34 (47) (2022) e2205614.

[57] V. Sorokin, K. Vickneson, T. Kofidis, C.C. Woo, X.Y. Lin, R. Foo, C.M. Shanahan, Role of vascular smooth muscle cell plasticity and interactions in vessel wall inflammation, Front. Immunol. 11 (2020) 599415.

[58] E.P. Tracy, V. Stielberg, G. Rowe, D. Benson, S.S. Nunes, J.B. Hoying, W.L. Murfee, A.J. LeBlanc, State of the field: cellular and exosomal therapeutic approaches in vascular regeneration, Am. J. Physiol. Heart Circ. Physiol. 322 (4) (2022) H647-h680.

[59] W. Wystrychowski, S.A. Garrido, A. Marini, N. Dusserre, S. Radochonski, K. Zagalski, J. Antonelli, M. Canalis, A. Sammartino, Z. Darocha, R. Baczyński, T. Cierniak, H. Regele, L.M. de la Fuente, L. Cierpka, T.N. McAllister, N. L'Heureux, Long-term results of autologous scaffold-free tissue-engineered vascular graft for hemodialysis access, J. Vasc. Access (2022) 11297298221095994.

[60] M. Tennant, A. Barker, A.E. Storrie, J.K. McGeachie, Novel microsurgical model of experimental vascular neointimal hyperplasia, Microsurgery 14 (2) (1993) 102–106.

[61] H. Bai, H. Hu, J. Guo, M. Ige, T. Wang, T. Isaji, T. Kudze, H. Liu, B. Yatsula, T. Hashimoto, Y. Xing, A. Dardik, Polyester vascular patches acquire arterial or venous identity depending on their environment, J. Biomed. Mater. Res. A 105 (12) (2017) 3422–3431.

[62] H. Bai, P. Sun, H. Wu, S. Wei, B. Xie, W. Wang, Y. Hou, J. Li, A. Dardik, Z. Li, The application of tissue-engineered fish swim bladder vascular graft, Commun. Biol. 4 (1) (2021) 1153.

[63] P. Sun, S. Yan, L. Zhang, C. Zhang, H. Wu, S. Wei, B. Xie, X. Wang, H. Bai, Egg shell membrane as an alternative vascular patch for arterial angioplasty, Front. Bioeng. Biotechnol. 10 (2022) 843590.

[64] F. Kawecki, N. L'Heureux, Current biofabrication methods for vascular tissue engineering and an introduction to biological textiles, Biofabrication 15 (2) (2023).

[65] M. Itoh, K. Nakayama, R. Noguchi, K. Kamohara, K. Furukawa, K. Uchihashi, S. Toda, J. Oyama, K. Node, S. Morita, Scaffold-free tubular tissues created by a bio-3D printer undergo remodeling and endothelialization when implanted in rat aortae, PLoS One 10 (9) (2015) e0136681.

[66] Y. Li, Y. Zhou, W. Qiao, J. Shi, X. Qiu, N. Dong, Application of decellularized vascular matrix in small-diameter vascular grafts, Front. Bioeng. Biotechnol. 10 (2022) 1081233.

[67] S. Pashneh-Tala, S. MacNeil, F. Claeyssens, The tissue-engineered vascular graft-past, present, and future, Tissue Eng. Part B Rev. 22 (1) (2016) 68–100.

[68] D. Durán-Rey, V. Crisóstomo, J.A. Sánchez-Margallo, F.M. Sánchez-Margallo, Systematic review of tissue-engineered vascular grafts, Front. Bioeng. Biotechnol. 9 (2021) 771400.